Formation and Subduction of Central Mode Water Based on Profiling Float Data, 2003–08

EITAROU OKA,*,+ SHINYA KOUKETSU,+ KATSUYA TOYAMA,# KAZUYUKI UEHARA,@ TAIYO KOBAYASHI,+ SHIGEKI HOSODA,+ AND TOSHIO SUGA+,#

* *Atmosphere and Ocean Research Institute, The University of Tokyo, Kashiwa, Japan*
+ *Research Institute for Global Change, Japan Agency for Marine-Earth Science and Technology, Yokosuka, Japan*
# *Department of Geophysics, Graduate School of Science, Tohoku University, Sendai, Japan*
@ *Department of Marine Science, School of Marine Science and Technology, Tokai University, Shizuoka, Japan*

(Manuscript received 24 December 2009, in final form 18 August 2010)

ABSTRACT

Temperature and salinity data from Argo profiling floats in the North Pacific during 2003–08 have been analyzed to study the structure of winter mixed layer north of the Kuroshio Extension and the subsurface potential vorticity distribution in the subtropical gyre in relation to the formation and subduction of the central mode water (CMW). In late winter, two zonally elongated bands of deep mixed layer extend at 33°–39° and 39°–43°N, from the east coast of Japan to 160°W. These correspond to the formation region of the lighter variety of CMW (L-CMW) and that of the denser variety of CMW (D-CMW) and the recently identified transition region mode water (TRMW), respectively. In the western part of the L-CMW and D-CMW–TRMW formation regions west of 170°E, the winter mixed layer becomes deeper and lighter to the east (i.e., to the downstream). As a result, the formed mode water is reentrained into the mixed layer in the farther east in the following winter and modified to the lighter water and is thus unable to be subducted to the permanent pycnocline. In the eastern part of the formation regions between 170°E and 160°W, on the other hand, the winter mixed layer becomes shallower and lighter to the east. From these areas, the L-CMW with potential density of 25.7–26.2 kg m^{-3} and the D-CMW–TRMW (mostly the former) of 26.1–26.4 kg m^{-3} are subducted to the permanent pycnocline, and they are then advected anticyclonically in the subtropical gyre. These results imply that during the analysis period large-scale subduction to the permanent pycnocline occurs in the density range up to 26.4 kg m^{-3} in the open North Pacific, whereas the winter mixed layer density reaches the maximum of 26.6 kg m^{-3}. This is supported by the vertical distribution of apparent oxygen utilization in a hydrographic section in the subtropical gyre.

1. Introduction

Central mode water (CMW) is characterized by a pycnostad lying in the lower ventilated pycnocline in the North Pacific subtropical gyre. Motivated by Talley's (1988) potential vorticity (Q) map on the σ_θ = 26.2 kg m^{-3} isopycnal (σ_θ is potential density) indicating a horizontal Q minimum in the central part of the gyre, Nakamura (1996) and Suga et al. (1997) separately identified a thermostad of 8.5°–11.5° and 10°–13°C using different climatological data and termed it CMW. Recent isopycnal Q maps of Suga et al. (2004), which are based on the isopycnally averaged North Pacific HydroBase climatology (Macdonald et al. 2001), delineate that the low-Q signature of CMW extends anticyclonically from the northern to western boundary of the subtropical gyre on isopycnals between σ_θ = 25.9 and 26.5 kg m^{-3}.

The distribution and properties of CMW are observed to change on decadal and interdecadal time scales (Yasuda and Hanawa 1997; Suga et al. 2003). Therefore, the CMW circulation in the subtropical gyre can cause the observed and modeled propagation of temperature anomalies in the permanent pycnocline (e.g., Deser et al. 1996; Schneider et al. 1999; Nonaka et al. 2000), which might be important for decadal–interdecadal climate variability in the Pacific region (Latif and Barnett 1994; Gu and Philander 1997). CMW also possibly affect the long-term climate variability by transporting anthropogenic carbon both downward and meridionally because the formation region of CMW,

Corresponding author address: Eitarou Oka, Atmosphere and Ocean Research Institute, The University of Tokyo, Kashiwa, Chiba 277-8564, Japan.
E-mail: eoka@aori.u-tokyo.ac.jp

DOI: 10.1175/2010JPO4419.1

described in detail below, is an intense sink for atmospheric CO_2 (e.g., Takahashi et al. 2009).

CMW is formed in the deep winter mixed layer[1] north of the Kuroshio Extension (Ladd and Thompson 2000; Suga et al. 2004; Oka et al. 2007; Ohno et al. 2009). An analysis of data from a repeat hydrographic section along 165°E during 1991–2003 (Oka and Suga 2005) demonstrated that a lighter (denser) variety of CMW with σ_θ = 25.8–26.2 (26.3–26.4) kg m^{-3} is formed between the Kuroshio Extension and its northern bifurcation (the northern bifurcation and the subarctic front[2]). The differential formation of CMW was also observed in a hydrographic section along 179°E (Mecking and Warner 2001) and was reproduced in a high-resolution ocean general circulation model (Tsujino and Yasuda 2004).

The CMW formation region was initially inferred to extend zonally from 175°E to 160°W based on Suga et al.'s (1997) temperature climatology, but more recent data have demonstrated that the formation region extends much farther westward. The ever presence of CMW in the 165°E repeat section and the surrounding flow field (generally eastward) imply that the formation region extends at least as far west as 155°E (Oka and Suga 2005). Furthermore, upgraded winter mixed layer climatology of Suga et al. (2004) demonstrated that the probable formation region of CMW, which is defined as the winter mixed layer having the same potential temperature and salinity as the CMW pycnostads in the permanent pycnocline, extends as far west as 143°E, almost reaching the east coast of Japan.

How is CMW subducted from this zonally elongated formation region into the permanent pycnocline? The mechanism is important in determining the CMW properties and causing their variability but has not been well clarified. Numerical models demonstrated that CMW is subducted east of the date line by crossing a sharp front of the mixed layer depth (MLD) at the eastern end of the formation region (e.g., Kubokawa and Inui 1999; Xie et al. 2000; Hosoda et al. 2004; Tsujino and Yasuda 2004). On the other hand, climatological data indicated that the water is mainly subducted from a wide area in the formation region where the winter MLD gradually decreases eastward while the mixed layer density changes little (Suga et al. 2004, 2008). Ladd and Thompson (2000) and Mecking and Warner (2001) speculated that the CMW formed in the western part of the formation region is not subducted into the permanent pycnocline but reentrained into the mixed layer in the following winters, thereby preconditioning the subduction in the eastern part of the formation region. That is, the eastward subsurface advection of low Q from the western part and the resultant weak density stratification below the seasonal pycnocline in the eastern part enable the winter mixed layer there to deepen to a considerable depth in spite of relatively weak surface cooling.

The CMW subduction mechanism so far has been investigated using climatological data by most of the previous studies, but these analyses had intrinsic difficulties (Suga et al. 2004). If we suppose a synoptic Q map on an isopycnal in the CMW density range, the lowest Q of CMW immediately after subduction should be located just south or east of the winter outcrop of the isopycnal, neighboring high Q in the seasonal pycnocline on the other side of the outcrop. The smoothing process of climatology inevitably averages these low and high Q across the winter outcrop, thus considerably weakening the low-Q signature of CMW. In fact, Suga et al. (2004) demonstrated that the most upstream portion of CMW on each isopycnal is not directly connected to the winter outcrop, even though they employed as small smoothing scale as possible for their climatology. The low Q of the CMW in the formation region should also be vulnerable to the smoothing process because of its meridional extent of only a few degrees in latitude (Oka and Suga 2005). In addition, the winter MLD in the formation region tends to be overestimated because the smoothing process mixes different water types across the subarctic front, causing artificial cabbeling in the surface layer (Ohno et al. 2004; Suga et al. 2004). It is thus suggested that we need to reexamine the CMW subduction mechanism using in situ observation data unaffected by the smoothing process.

Since 2000, profiling floats have been deployed in the global ocean under the international Argo program (Roemmich et al. 2001). The unprecedented array of 3000 floats, which has a horizontal resolution of 3° in latitude and longitude, was completed in 2007 (Roemmich et al. 2009) and is providing temperature and salinity data down to 2000-dbar depth in near–real time with relatively small regional biases and almost no seasonal bias. In this study, we analyze the float data in the North Pacific during 2003–08 to investigate the detailed structure of winter mixed layer north of the Kuroshio Extension and the subsurface Q distribution in the subtropical gyre in relation to the CMW formation and subduction. By using the unsmoothed

[1] In this study, the term mode water indicates a pycnostad lying in the subsurface during the warm season as well as that outcropping to the sea surface in late winter (i.e., deep winter mixed layer). The formation of such deep winter mixed layer is referred to as the formation of a mode water. The subduction of a mode water means a situation in which a mode water or part of it is advected into the permanent pycnocline during the warm season and is not reentrained into the mixed layer in the subsequent winters. The subduction occurs in the whole or part of the formation region of the mode water.

[2] In this study, the term subarctic front is used for a density-compensating front between the warmer, saltier water in the subtropical gyre and the colder, fresher water in the subarctic gyre (Roden 1970, 1972; Zhang and Hanawa 1993; Yuan and Talley 1996). Some studies refer to this front as the subarctic boundary (e.g., Favorite et al. 1976; Yasuda 2003).

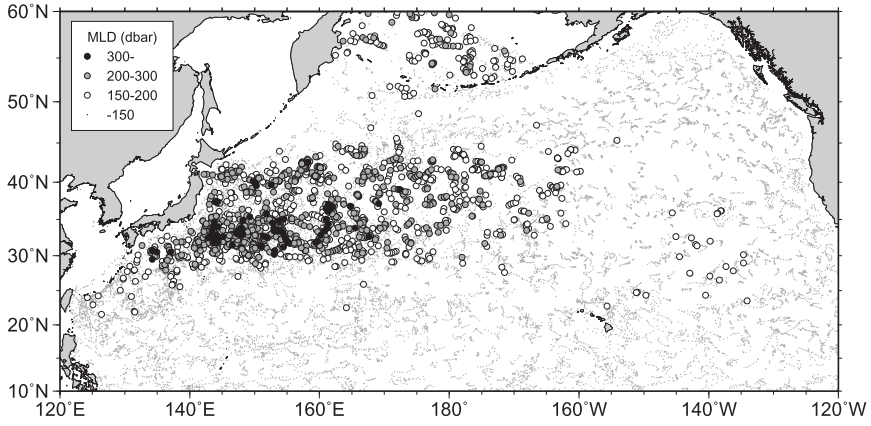

FIG. 1. Distribution of MLD in February–April of 2003–08.

float data, we will demonstrate a direct connection between the deep winter mixed layer and the subsurface low Q, clarifying the location and mechanism of the CMW subduction. Note that in this study we will not consider interannual variation of the CMW formation–subduction during the analysis period. It would be ideal to do the present analysis using float data from a single year, but their spatial density is not enough to resolve the detailed structure of winter mixed layer in the CMW formation region (Bingham and Suga 2006).

The reminder of this paper is organized as follows: The data and their processing are explained in section 2. In section 3, the winter mixed layer structure around the CMW formation region is investigated using late winter float data, from which the CMW subduction mechanism is inferred. The inferred mechanism is verified in section 4, by examining the CMW circulation in the subtropical gyre using float data during the warm season. Summary and discussion are given in section 5.

2. Data and processing

We used temperature (T) and salinity (S) data obtained by Argo profiling floats in the North Pacific in 2003–08. These floats drift freely at a predetermined parking pressure (typically 1000 dbar), and conduct T–S measurements between near the sea surface (4 dbar) and an intermediate depth (2000 dbar) at a predetermined interval (10 days). The collected data at about 70–120 sampling pressures, with a typical interval of 5 dbar at depths shallower than 200 dbar, 10–25 dbar at 200–1000 dbar, and 50–100 dbar at deeper than 1000 dbar, are transmitted from the surfaced floats to satellites and are made freely available within 24 h, after passing through the Argo real-time quality control (Argo Data Management Team 2009).

We downloaded the real-time quality controlled float data from the ftp site of Argo Global Data Assembly Center (available online at ftp://usgodae1.fnmoc.navy.mil/pub/outgoing/argo; ftp://ftp.ifremer.fr/ifremer/argo) and eliminated defective T–S profiles, such as those with measurements flagged as bad and those lacking intermediate layers for certain depths, following the procedures of Oka et al. (2007). Then we interpolated each T–S profile on a one-dbar grid using the Akima spline (Akima 1970) and calculated potential temperature (θ), σ_θ, and Q. Here, Q is defined as

$$Q = -\frac{f}{\rho}\frac{\partial \sigma_\theta}{\partial z}, \tag{1}$$

where f is the Coriolis parameter, ρ is in situ water density, and z is the vertical coordinate (positive upward). In Eq. (1), relative vorticity is neglected because it is comparable to planetary vorticity only in the vicinity of the Kuroshio Extension and other strong currents' axis (e.g., Qiu et al. 2006), whereas deep winter mixed layers are typically formed between such currents.

MLD is defined as the shallower value of the depth at which σ_θ increases by 0.03 kg m^{-3} from the sea surface and at which θ decreases or increases by 0.2°C from the surface, following the definition of Oka et al. (2007). Values of θ, S, and σ_θ at 10 dbar were used as the surface values and were considered to represent those of the mixed layer.

3. Structure of winter mixed layer in the CMW formation region

Using the 6-yr float data, an MLD map in the North Pacific is constructed for three late winter months of February–April, during which MLDs in the CMW formation region reach their maximum (Oka et al. 2007; Fig. 1). The MLD map indicates three regions exceeding 150 dbar, as demonstrated in previous studies (e.g., Kara et al. 2000; Suga et al. 2004; Ohno et al. 2009). The largest

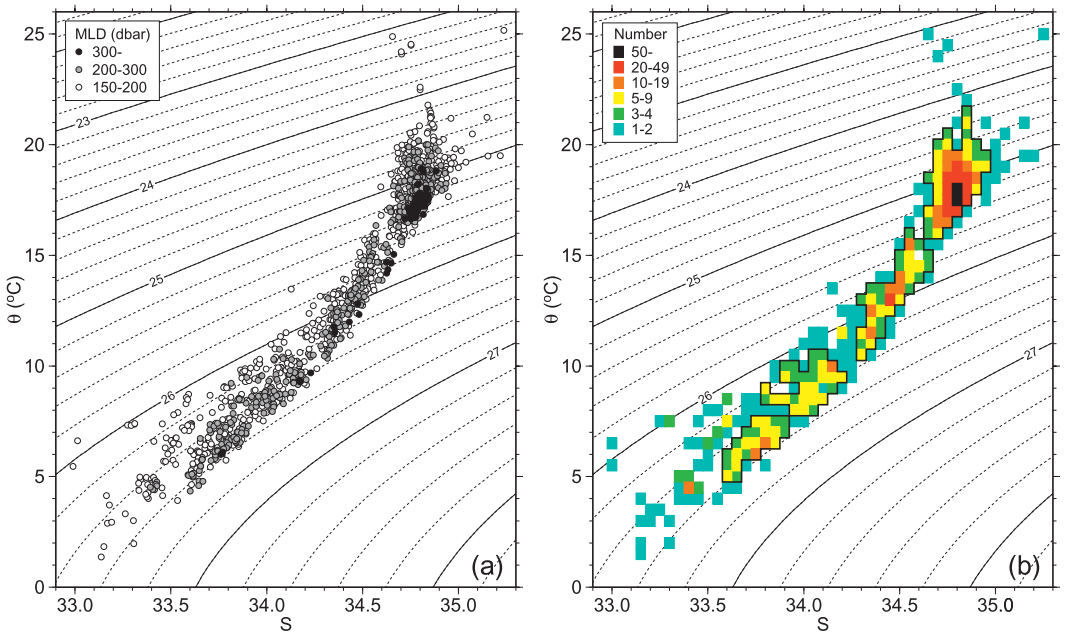

FIG. 2. (a) The θ–S relationship for the mixed layer deeper than 150 dbar in the western and central midlatitude North Pacific in February–April of 2003–08. Symbol types indicate MLD. (b) Number of points in (a), classified for each 0.05 (S) × 0.5° (θ) bin. Thick black lines indicate properties of mode waters. In both (a) and (b), solid and dashed contours denote σ_θ (kg m^{-3}).

one with the deepest mixed layers spreads widely in the western and central part of the midlatitude North Pacific. The second one is located in the deep basin of the Bering Sea and south of the Aleutian Islands, where the lower part of the winter mixed layer remains in the subsurface as the dichothermal water in the following seasons (e.g., Dodimead et al. 1963; Miura et al. 2002; Ueno et al. 2005). The smallest one with the shallowest mixed layers among the three regions lies in the eastern North Pacific Transition Region Mode Water near 30°N, 140°W, which corresponds to the formation region of the North Pacific Eastern Subtropical Mode Water (Hautala and Roemmich 1998). Because CMW is formed in the largest region in the western and central midlatitude North Pacific, we will concentrate on the winter mixed layer there hereafter.

The deep winter mixed layer in the region exhibits a near-linear, continuous θ–S relation between 5° and 20°C (Fig. 2a). In this diagram, outcropping mode waters, namely the deep winter mixed layer having common θ–S and a large horizontal extent, are expected to appear as concentrations of points because of relatively uniform distribution of the profiling float observations (Fig. 1). To detect mode waters, the number of points in Fig. 2a are counted for each bin of $\theta \times S$ (Fig. 2b) and θ and S (Figs. 3a,b). A pronounced maximum is found around $\theta = 18.0$°C and $S = 34.80$, which are the typical properties of the North Pacific Subtropical Mode Water (STMW; Masuzawa 1969).

On the colder and fresher side of the maximum for STMW, there seem to be three smaller maxima around $\theta =$ 13.0°, 9.0°, and 6.5°C and $S = 34.45$, 34.05, and 33.80 in each of Figs. 2b and 3a,b. When we compose groups of adjacent θ–S bins with three or more float observations, as indicated by thick black lines in Fig. 2b, the properties of each group agree with the previously reported properties of a mode water. That is, the warmest group (θ = 16.0°–21.5°C, S = 34.65–34.95, and σ_θ = 24.2–25.6 kg m^{-3}) corresponds to STMW; the second and third groups (10.5°–16.0°C, 34.30–34.65, and 25.4–26.3 kg m^{-3}; 8.0°–10.5°C, 33.80–34.20, and 26.1–26.5 kg m^{-3}) correspond to the lighter CMW (L-CMW) and denser CMW (D-CMW) observed in the 165°E repeat section (Oka and Suga 2005); and the coldest group (5.0°–7.5°C, 33.60–33.90, and 26.4–26.6 kg m^{-3}) corresponds to the recently identified transition region mode water (TRMW; Saito et al. 2007), which is formed and distributed in the transition region north of the subarctic front in the western North Pacific. Consequently, we define the four mode waters in their formation regions using these four groups of θ–S bins.

Although the four mode waters have distinct θ and S, the σ_θ of L-CMW, D-CMW, and TRMW is relatively close to each other, particularly between the latter two. As a result, number of float observations for each σ_θ bin exhibits only two peaks: one peak at 24.8–25.5 kg m^{-3} for STMW and the other peak at 25.8–26.6 kg m^{-3} for the remaining three mode waters (Fig. 3c). This implies that

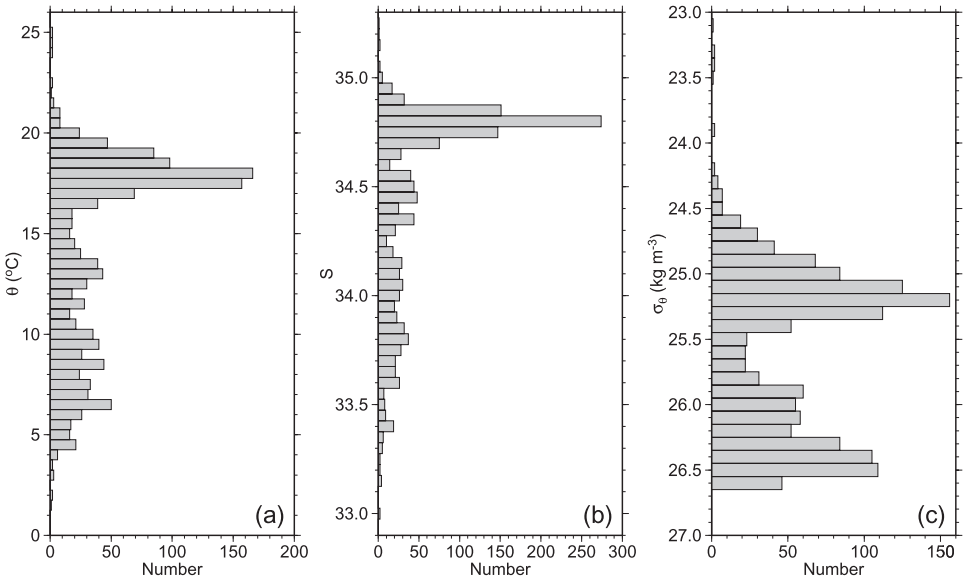

FIG. 3. Number of points in Fig. 2a, classified for each (a) 0.5° bin of θ, (b) 0.05 bin of S, and (c) 0.1 kg m^{-3} bin of σ_θ. Note that σ_θ increases downward on the ordinate in (c).

the three mode waters cannot be distinguished from each other by means of σ_θ only. It should be also mentioned that no deep winter mixed layer is observed on the denser side of the 25.8–26.6 kg m^{-3} peak; 26.6 kg m^{-3} is the densest σ_θ class in the western and central midlatitude North Pacific, as demonstrated in previous studies (e.g., Talley 1993).

The formation regions of the four mode waters are mapped in Fig. 4. The STMW formation region lying in the recirculation gyre south of the Kuroshio and the Kuroshio Extension is located between 26° and 36°N, with a somewhat larger horizontal extent than demonstrated in previous studies (e.g., Oka and Suga 2003; Oka 2009) because of the wider θ–S range used for the STMW definition in this study. To the north of the Kuroshio Extension, the L-CMW formation region extends zonally between 143°E and 163°W at 33°–39°N, shifting gradually southward toward the east. In the farther north, the formation regions of D-CMW and TRMW mingle with each other at 39°–43°N, also extending zonally from 142°E to 160°W. In this latitude band, both D-CMW and TRMW are formed between 148° and 178°E, whereas only TRMW (D-CMW) is formed west (east) of it. Thus, the two zonal bands of the L-CMW and D-CMW–TRMW formation regions extend from the east coast of Japan to 160°W for roughly 5000 km.

The geopotential anomaly distribution in Fig. 4 denotes that the subsurface geostrophic flow in these regions is generally eastward with a speed of ~3 cm s^{-1}, which is equivalent to ~10° in longitude per year. Therefore, in each of the L-CMW and D-CMW–TRMW formation regions, the mode water is expected to be advected eastward, spending about 5 yr from the western to the eastern end of the region. During this journey, the properties of mode water are likely to be altered by various processes, such as the surface heat and freshwater fluxes, detrainment–entrainment to and from the underlying layer, horizontal advection, mixing, etc., not only in late winter when deep mixed layer is formed but also in the other seasons.

In fact, the properties of each mode water change considerably eastward within the formation region (Fig. 5). The θ of L-CMW increases from ~11° to ~14°C, and its S slightly increases from ~34.4 to ~34.5, in contrast with the θ and S of STMW decreasing eastward. The θ and S increases of L-CMW are believed to be caused primarily by the northward component of geostrophic flow (this is indicated by a few streamlines joining the L-CMW formation region from the south; Fig. 4) that brings warmer and saltier water to the region, because other processes—such as the surface heat and evaporation minus precipitation fluxes that are both negative on the annual average in most part of the region (Fig. 6), the entrainment from the colder and fresher underlying layer, and the southward Ekman transport due to the prevailing westerlies—are all expected to decrease the θ and S of L-CMW. As a result of the eastward θ increase, the σ_θ of L-CMW in the formation region decreases from ~26.3 to ~25.7 kg m^{-3} (Fig. 5c).

The θ of D-CMW in the formation region increases eastward from ~8° to ~10°C, whereas its S decreases from ~34.1 to ~33.9 (Figs. 5a,b). TRMW is much colder

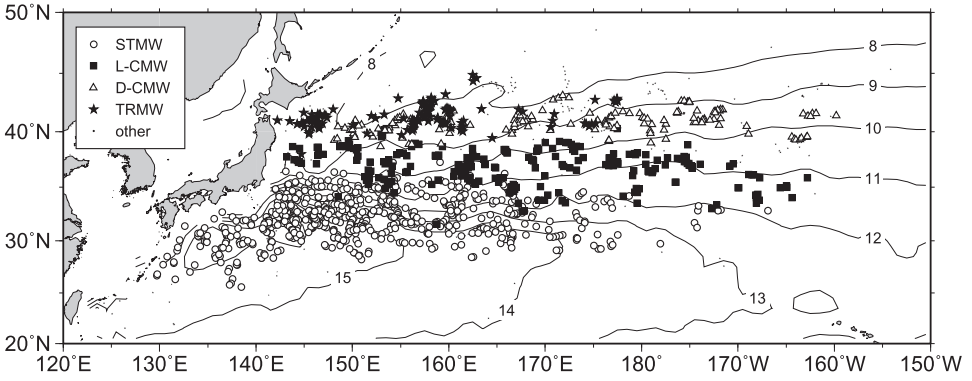

FIG. 4. Distributions of the mixed layer deeper than 150 dbar in the western and central midlatitude North Pacific with the properties of STMW (white circles), L-CMW (black squares), D-CMW (white triangles), and TRMW (black stars) and without the mode water properties (dots) in February–April of 2003–08. Contours indicate geopotential anomaly ($m^2\ s^{-2}$) at 150 dbar relative to 950 dbar, calculated using the Argo profiling float data during 2003–08 and an optimal interpolation technique (Bretherton et al. 1976).

(~6°C) and fresher (~33.7) than D-CMW at the western end of the formation region, but its θ and S gradually increase and approach those of D-CMW toward the east and seem to merge into them near 180°. This structure is consistent with a recent analysis of Argo float data during 2001–05 (Saito 2006), which demonstrated that TRMW is modified to warmer and saltier D-CMW within approximately a year from its formation in winter. This occurs because after spring geostrophic flow with a vertical shear from the south brings the warmer, saltier, and equally dense water to the surface layer of the TRMW formation region, leading to double-diffusive salt-finger convection between the surface water and the underlying TRMW that increases the θ and S of TRMW (Saito 2006). Such modification would provide a precondition favorable to the formation of more D-CMW than TRMW to the downstream, possibly leading to the termination of TRMW formation near the date line.

The downstream θ increase of D-CMW and TRMW is also likely to be due to the northward geostrophic advection into the formation region of these waters (Fig. 4), whereas the S decrease of D-CMW cannot be explained by the same mechanism. In the D-CMW formation region, the salinity input by the geostrophic advection is probably exceeded by the surface freshwater flux that is much stronger than in the L-CMW formation region (Fig. 6b) and the southward Ekman transport that brings much fresher water of the transition region. The TRMW to D-CMW modification explained above would also dilute D-CMW.

The σ_θ of D-CMW in the formation region decreases eastward from ~26.5 to ~26.1 kg m^{-3} because of the θ increase and S decrease (Fig. 5). TRMW is slightly denser than D-CMW, and it also decreases its σ_θ from ~26.6 to ~26.4 kg m^{-3} because of the θ increase. As a result of the large zonal σ_θ changes of L-CMW and D-CMW, the D-CMW in the easternmost part of the formation region is comparably as dense as or even lighter than the L-CMW in the westernmost part of the formation region, although both θ and S are significantly different between these waters. Such property distribution is reflected in the single peak for L-CMW, D-CMW, and TRMW in the σ_θ-based observation number histogram (Fig. 3c) and the three individual peaks for the three waters in the θ- and S-based histograms (Figs. 3a,b).

The late winter MLD also exhibits significant zonal variation within each mode water formation region (Fig. 7). The MLD in the STMW formation region is at a maximum between 140° and 150°E, where the southern recirculation of the Kuroshio Extension is strongest (e.g., Qiu and Chen 2005). The MLD in the L-CMW formation region is largest farther east near 170°E, decreasing to both the west and the east, except for some large values west of 155°E that might be related to anticyclonic mesoscale eddies. This means that the MLD in the L-CMW formation region increases to the downstream in the western part of the region and decreases in the eastern part, possibly because of intense winter cooling in the western part and milder cooling in the eastern part (Fig. 6a). The MLD in the D-CMW–TRMW formation region presents a similar structure to the L-CMW formation region; it slightly increases to the downstream in the western part and gradually decreases in the eastern part, reaching the maximum near 170°E (Fig. 7c). In both the L-CMW and D-CMW–TRMW formation regions, the eastward MLD decrease in the eastern part is gradual without any sharp MLD front, as in the climatological MLD field (Suga et al. 2004, 2008).

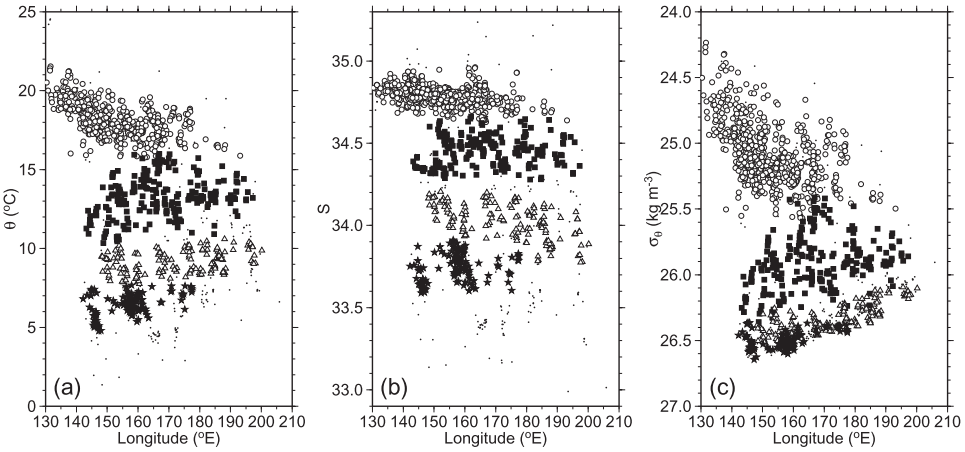

FIG. 5. Plots of (a) θ, (b) S, and (c) σ_θ against longitude for the mixed layer deeper than 150 dbar in the western and central midlatitude North Pacific in February–April of 2003–08. The symbols follow Fig. 4. Note that σ_θ increases downward on the ordinate in (c).

What subduction scheme can be inferred for L-CMW and D-CMW–TRMW from the observed mixed layer and current structures in their formation regions (Figs. 4, 5, 7)? In the western part of the formation regions west of 170°E where the winter mixed layer becomes deeper and lighter to the downstream, it is expected that the lower portion of the winter mixed layer remains in the subsurface as low-Q water in spring to summer, and it is then reentrained into the mixed layer in the following winter about 10° in longitude to the east. On the other hand, in the eastern part of the formation regions east of 170°E where the winter mixed layer becomes shallower and lighter to the downstream, the lower portion of the winter mixed layer is unlikely to be reentrained into the mixed layer in the farther east in the following winters, thereby being subducted into the permanent pycnocline. If this occurs, the mixed layer density distribution in Fig. 5c implies that the L-CMW with σ_θ = 25.7–26.2 kg m^{-3} and the D-CMW–TRMW with 26.1–26.4 kg m^{-3} are subducted from the eastern part of the formation regions between 170°E and 160°W, whereas the L-CMW with 26.3 kg m^{-3} and the D-CMW–TRMW with 26.5–26.6 kg m^{-3} that exist only in the western part of the formation region are not subducted to the permanent pycnocline. In the next section, we will demonstrate that this subduction scheme is basically correct, by examining the subsurface CMW circulation in the subtropical gyre.

The above scheme implies that in the western part of the formation region the CMW left in the subsurface during the warm season is reentrained into the mixed layer having slightly lower density in the following winter. This scenario might seem surprising, but it is confirmed by Lagrangian observations performed by several Argo profiling floats. One example is obtained by a float that drifts eastward around 41°N in the D-CMW–TRMW formation region at a speed[3] of about 10° in longitude per year (Fig. 8).

In summer 2007, low Q ($<1.5 \times 10^{-10}$ m^{-1} s^{-1}) of D-CMW with σ_θ = 26.5 kg m^{-3}, which is presumably formed in late winter 2007 in the farther west, is seen at depths of 150–250 dbar below high Q ($>5 \times 10^{-10}$ m^{-1} s^{-1}) of the seasonal pycnocline. In October, the depth and σ_θ of the mixed layer start increasing and finally reach the maximum of 292 dbar and 26.43 kg m^{-3} on 10 March 2008. During this period, the depth and σ_θ of the seasonal pycnocline beneath the mixed layer also increase while its Q decreases. In association with these deepenings, the low Q of D-CMW gradually weakens at σ_θ = 26.5 kg m^{-3}, presumably because of reentrainment to the overlying seasonal pycnocline enhanced by mechanical mixing, and it is finally replaced by relatively high Q ($>3 \times 10^{-10}$ m^{-1} s^{-1}) just beneath the developed mixed layer in February. After the mixed layer shallows in March and April, low Q of newly formed D-CMW is left in the subsurface at σ_θ = 26.4 kg m^{-3}, while Q at σ_θ = 26.5 kg m^{-3} is not low anymore. Thus, through the winter season, the D-CMW lying in the subsurface in the western part of the formation region is reentrained into the slightly lighter winter mixed layer, which is then left in the subsurface as newly formed D-CMW.

4. CMW circulation in the subtropical gyre

In most of the previous studies, the CMW circulation in the subtropical gyre has been examined using climatological

[3] This speed happens to coincide with the eastward advection speed at 150 dbar in the CMW formation region estimated from Fig. 4, although the float drifts at a parking pressure of 1000 dbar.

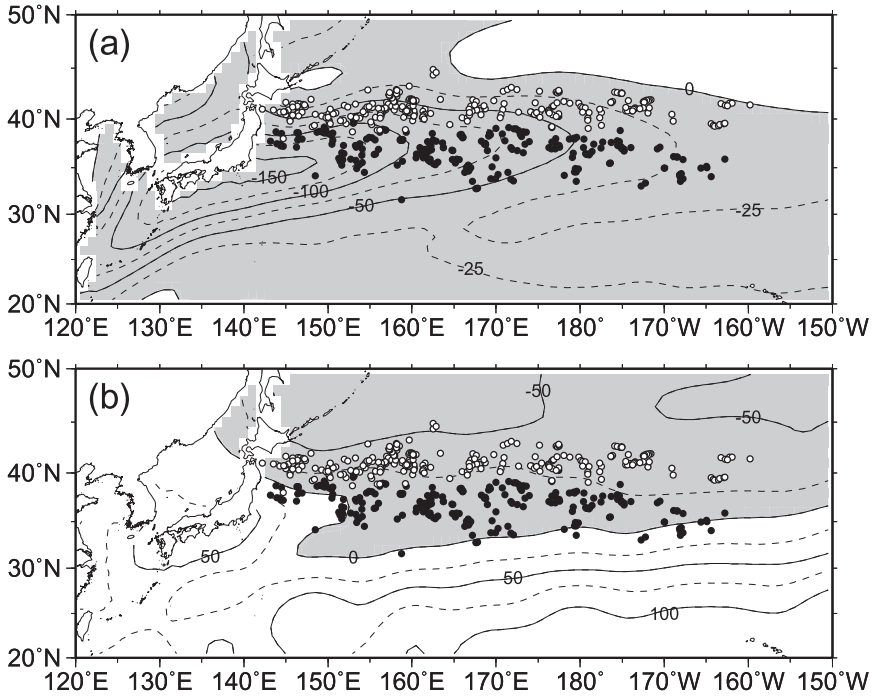

FIG. 6. Annual-mean (a) net surface heat flux (W m^{-2}) and (b) evaporation minus precipitation flux (cm yr^{-1}), calculated using monthly climatologies of surface heat and freshwater fluxes and wind stress from da Silva et al. (1994). The fluxes are positive when the ocean gains heat and loses freshwater. Negative values are shaded. Dots (circles) denote the formation regions of L-CMW (D-CMW–TRMW).

data, which do not properly represent the CMW structure around the formation region (section 1). The alternative use of in situ observation data from Argo profiling floats is expected to provide a better view, but simply averaging Q values from the float data at each location could also mar the low-Q structure of CMW around the formation region, as in the climatological cases. We therefore calculated the frequency of low Q at each location on the isopycnals between σ_θ = 25.7 and 26.6 kg m^{-3} for the warm season of 2003–08 (Fig. 9), based on which the CMW subduction scheme proposed in the previous section is verified. It should be noted that the following results do not depend on the choice of critical Q value for each isopycnal.

On the isopycnal of σ_θ = 26.6 kg m^{-3}, the frequency of low Q is high around 40°–42°N, 152°–163°E, which lies in the D-CMW–TRMW formation region (Fig. 4). This low-Q patch is considered to represent TRMW that is formed at 145°–160°E in winter (Fig. 5c) and then advected eastward to the observed location. The low-Q patch, however, does not extend to the downstream anymore; the frequency drops to less than 10% east of 170°E (Fig. 9). This discontinuity implies that the TRMW lying at 152°–163°E in spring to summer is reentrained into the mixed layer in the following winter in the farther east and modified to lighter TRMW or D-CMW, as demonstrated by the Lagrangian float observations (Fig. 8). The same applies to D-CMW–TRMW with σ_θ = 26.5 kg m^{-3}, which is formed at 145°–165°E in winter (Fig. 5c) and advected to 156°–174°E in spring to summer but disappears in the farther east (Fig. 9). Thus, the D-CMW–TRMW with σ_θ = 26.5–26.6 kg m^{-3} is not subducted to the permanent pycnocline, in spite of its abundance in the formation region (Fig. 3c).

The low-Q frequency on σ_θ = 26.4 kg m^{-3} exhibits a clearly different distribution from the denser isopycnals; the low Q extends anticyclonically from 41°N, 170°E to 18°N, 135°E while decreasing its intensity (Fig. 9). This indicates that D-CMW–TRMW with σ_θ = 26.4 kg m^{-3} is permanently subducted east of 170°E, and subsequently advected in the subtropical gyre toward the western boundary. On σ_θ = 26.3 kg m^{-3}, the low Q of D-CMW also extends anticyclonically from 40°N, 180° to the downstream. However, low Q is hardly seen in the upstream region west of 170°E, although the L-CMW with 26.3 kg m^{-3} is formed at 143°–155°E in winter (Fig. 5c). Because the L-CMW in the westernmost part of the formation region is relatively thin (Fig. 7b), its low Q might be dissipated quickly after spring.

On σ_θ = 26.2 kg m^{-3}, low Q departs from 41°N, 172°W in the D-CMW–TRMW formation region and from 37°N, 176°E in the L-CMW formation region, both

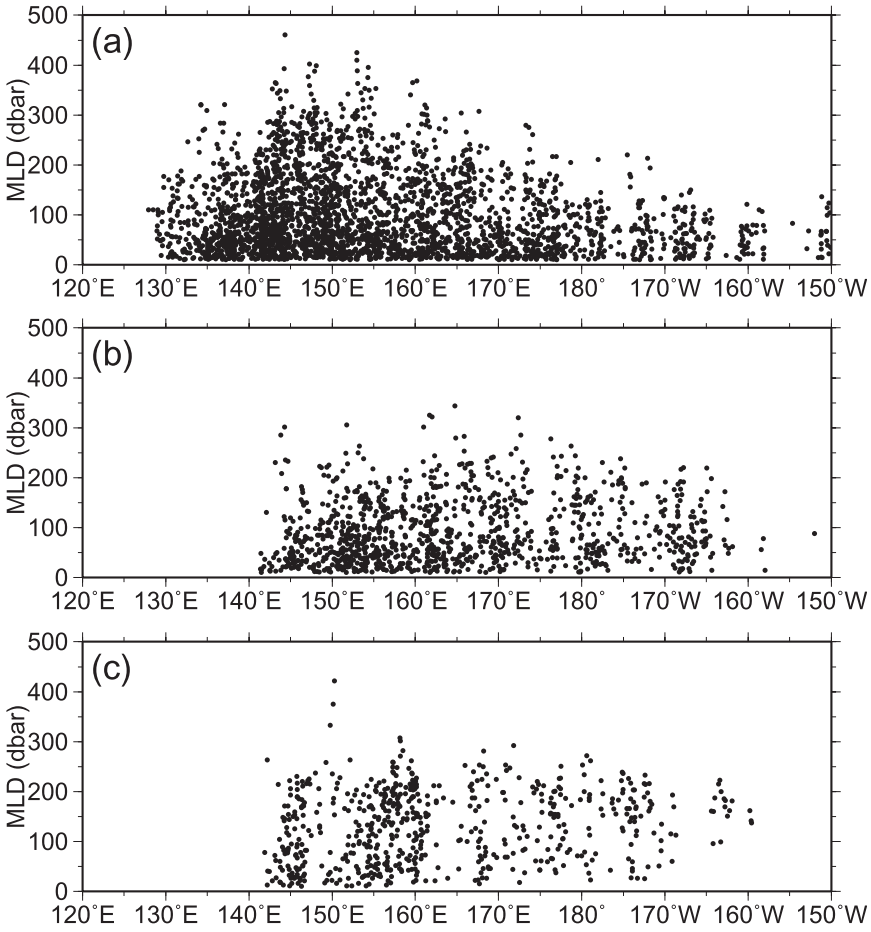

FIG. 7. Plots of MLD against longitude for the mixed layer in the western and central mid-latitude North Pacific with the properties of (a) STMW, (b) L-CMW, and (c) D-CMW–TRMW (defined in Fig. 2b) in February–April of 2003–08.

extending anticyclonically to the downstream. This isopycnal is ventilated by both varieties of CMW, which have the same density but significantly different θ–S (Fig. 5). The isopycnal of $\sigma_\theta = 26.1$ kg m^{-3} is also ventilated by both D-CMW and L-CMW, whose low Q extends from 38°N, 168°W and 36°N, 178°W, respectively (Fig. 9). On the lighter isopycnals of $\sigma_\theta = 25.7$–26.0 kg m^{-3}, low Q arises only from the L-CMW formation region at 33°–36°N, at a farther downstream location with decreasing σ_θ.

These features of the CMW circulation are summarized as follows. D-CMW–TRMW (L-CMW) with $\sigma_\theta = 26.1$–26.4 (25.7–26.2) kg m^{-3} is subducted to the permanent pycnocline around 40°–42°N (33°–37°N) east of 170°E and then extends anticyclonically in the subtropical gyre. The subduction point for each variety of CMW shifts eastward with decreasing σ_θ. On the other hand, D-CMW–TRMW with $\sigma_\theta = 26.5$–26.6 kg m^{-3}, whose low Q is confined to a relatively small area in the western part of the formation region, is not subducted to the permanent pycnocline but reentrained into the winter mixed layer and modified to the lighter water. The low Q on $\sigma_\theta = 26.5$–26.6 kg m^{-3} in the downstream region, which reappears near 30°N, 160°W and extends southwestward, is possibly supplied from the CMW on the lighter isopycnals through vertical diffusion. Thus, the subsurface CMW circulation represented by the low-Q frequency agrees well with that expected from the winter mixed layer and current structures. The most noticeable feature is the discontinuity of low Q on $\sigma_\theta = 26.5$–26.6 kg m^{-3}, which is not seen in the climatological Q maps (e.g., Suga et al. 2004). It should be emphasized that the CMW subduction actually occurs only in the eastern part of the formation region east of 170°E; the western part of the formation region preconditions the subduction in the eastern part, as speculated by Ladd and Thompson (2000) and Mecking and Warner (2001).

The confirmed CMW subduction scheme implies that during 2003–08 large-scale subduction to the permanent pycnocline occurs up to 26.4 kg m^{-3} in the open North Pacific, whereas the winter mixed layer density reaches the maximum of 26.6 kg m^{-3}. This should be reflected in

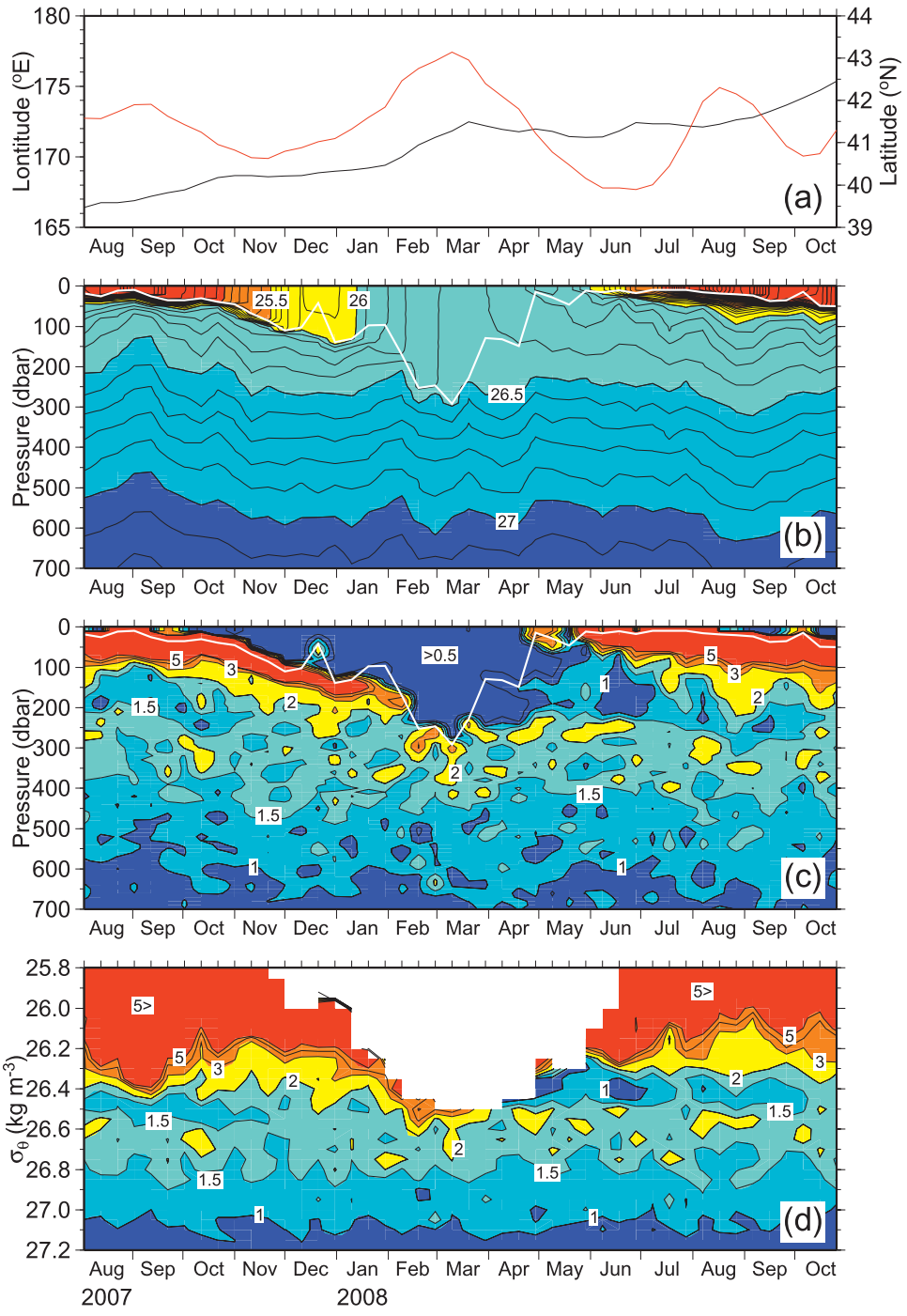

FIG. 8. (a) Time series of longitude (black curve) and latitude (red curve) obtained by an Argo profiling float with World Meteorological Organization identifier (WMO ID) 2900691 from 3 Aug 2007 through 26 Oct 2008. Time–pressure sections of (b) σ_θ (kg m^{-3}) and (c) Q (10^{-10} m^{-1} s^{-1}) and (d) time–σ_θ section of Q (10^{-10} m^{-1} s^{-1}) obtained by the same float as in (a). Contours are drawn at 0.5, 1, 1.5, 2, 3, 4, and 5×10^{-10} m^{-1} s^{-1} in (c) and (d). White curves in (b) and (c) denote MLD. Tick marks on the top of each panel indicate the float observations.

the distribution of chemical properties in the subtropical gyre. As the most comprehensive example, we here examine the vertical structure of apparent oxygen utilization (AOU) in the CMW distribution region, using conductivity–temperature–depth–oxygen ($CTDO_2$) data from the World Ocean Circulation Experiment Hydrographic Program (WHP) P02 section along 30°N in June–August 2004, downloaded from the WHP office Web site (see online at http://whpo.ucsd.edu). The P02 section exhibits two significant low-Q areas of mode waters embedded in high Q of the seasonal and permanent pycnoclines: one of STMW at $\sigma_\theta = \sim 25.4$ kg m^{-3} west of 180° and the other of CMW at 25.7–26.5 kg m^{-3} east of 175°E (Fig. 10). The AOU in the STMW is ~ 0.5 ml l^{-1}, which is low enough to indicate that the observed STMW is formed in the late winter of 2004 (Suga et al. 1989; Oka and Suga 2005).

The AOU in the CMW is also expected to be significantly lower than the underlying layers. To examine this relation, both Q and AOU were averaged at 33 $CTDO_2$ stations between 175° and 155°W where thick CMW is observed (Fig. 11). The average Q increases almost linearly upward at $\sigma_\theta > 26.6$ kg m^{-3} in the unventilated layer, and it shows negative anomalies at 25.7–26.6 kg m^{-3} in the CMW density range. The average AOU decreases upward above the AOU maximum at 27.3 kg m^{-3}. In the unventilated layer, $\partial \mathrm{AOU}/\partial\sigma_\theta$ is large and almost constant at 26.7–27.0 kg m^{-3}, but it decreases upward at $\sigma_\theta \leq$ 26.6 kg m^{-3} in the ventilated layer. The ventilated layer can be further divided by $\sigma_\theta = 26.3$ kg m^{-3} into the shallower layer with relatively low AOU and the deeper layer where AOU is high and greatly increases downward. This probably reflects primarily the difference in the subducted water volume between the two layers: that is, the difference that the shallower layer is heavily ventilated through the mode water formation, whereas the deeper layer is lightly ventilated because the formed mode waters are mostly reentrained into the mixed layer within a year.

5. Summary and discussion

Temperature and salinity data from Argo profiling floats in the North Pacific during 2003–08 have been analyzed to study the structure of winter mixed layer and the subsurface distribution of potential vorticity in relation to the formation and subduction of the central mode water (CMW). In late winter, two zonal bands of deep mixed layer extend north of the Kuroshio Extension at 33°–39° and 39°–43°N from the east coast of Japan to 160°W for roughly 5000 km. The mixed layer properties indicate that the southern band corresponds to the formation region of the lighter variety of CMW (L-CMW) and that the northern band corresponds to that of the denser variety of CMW (D-CMW) and the recently identified transition region mode water (TRMW). The subsurface geostrophic flow in these regions is generally eastward, with a small northward component.

Within the L-CMW (D-CWM–TRMW) formation region, the mixed layer density decreases eastward: that is, to the downstream, from 26.3 (26.6) to 25.7 (26.1) kg m^{-3}. The mixed layer depth in both regions increases to the downstream in the western part and gradually decreases in the eastern part, reaching the maximum at 170°E. As a result, the mode waters formed in the western part of the formation regions west of 170°E are reentrained into the mixed layer in the farther east in the following winter and modified to the lighter water, thus being unable to be subducted to the permanent pycnocline. In the eastern part of the formation regions between 170°E and 160°W, on the other hand, the L-CMW (D-CWM–TRMW) with potential density (σ_θ) of 25.7–26.2 (26.1–26.4) kg m^{-3} is subducted to the permanent pycnocline, and is then advected anticyclonically in the subtropical gyre. The subduction in the eastern part of the formation regions is preconditioned by the processes in the western part, as speculated by Ladd and Thompson (2000) and Mecking and Warner (2001).

These results imply that during the analysis period large-scale subduction to the permanent pycnocline occurs up to $\sigma_\theta = 26.4$ kg m^{-3} in the open North Pacific, whereas the mixed layer density reaches the maximum of 26.6 kg m^{-3}. This is largely supported by the vertical distribution of apparent oxygen utilization in a hydrographic section along 30°N. Earlier studies used maps of winter sea surface density and the Sverdrup streamfunction to demonstrate that the large-scale subtropical subduction is limited to σ_θ lower than 26.2 or 26.3 kg m^{-3} (Talley 1985), which could be modulated by the winter mixed layer structure (Woods 1985). In this study, we have clarified how this works in detail based on the float observations.

Although both D-CMW and TRMW are formed in the northern formation region, the TRMW formation is highly limited in the eastern part of the region east of 170°E where the subduction to the permanent pycnocline occurs (Figs. 4, 5). Therefore, little TRMW is believed to be subducted to the permanent pycnocline in spite of its abundance in the western part of the region. This probably explains partly the discrepancy in the volume distribution on the potential temperature–salinity (θ–S) diagram between the winter mixed layer and the lower ventilated pycnocline in the subtropical gyre: in other words, the reason why the water in the TRMW θ–S range does not produce a volumetric mode in the permanent pycnocline in the subtropical gyre, as argued by Suga et al. (2008).

In the repeat hydrographic section along 165°E, the L-CMW and D-CMW–TRMW formation regions are

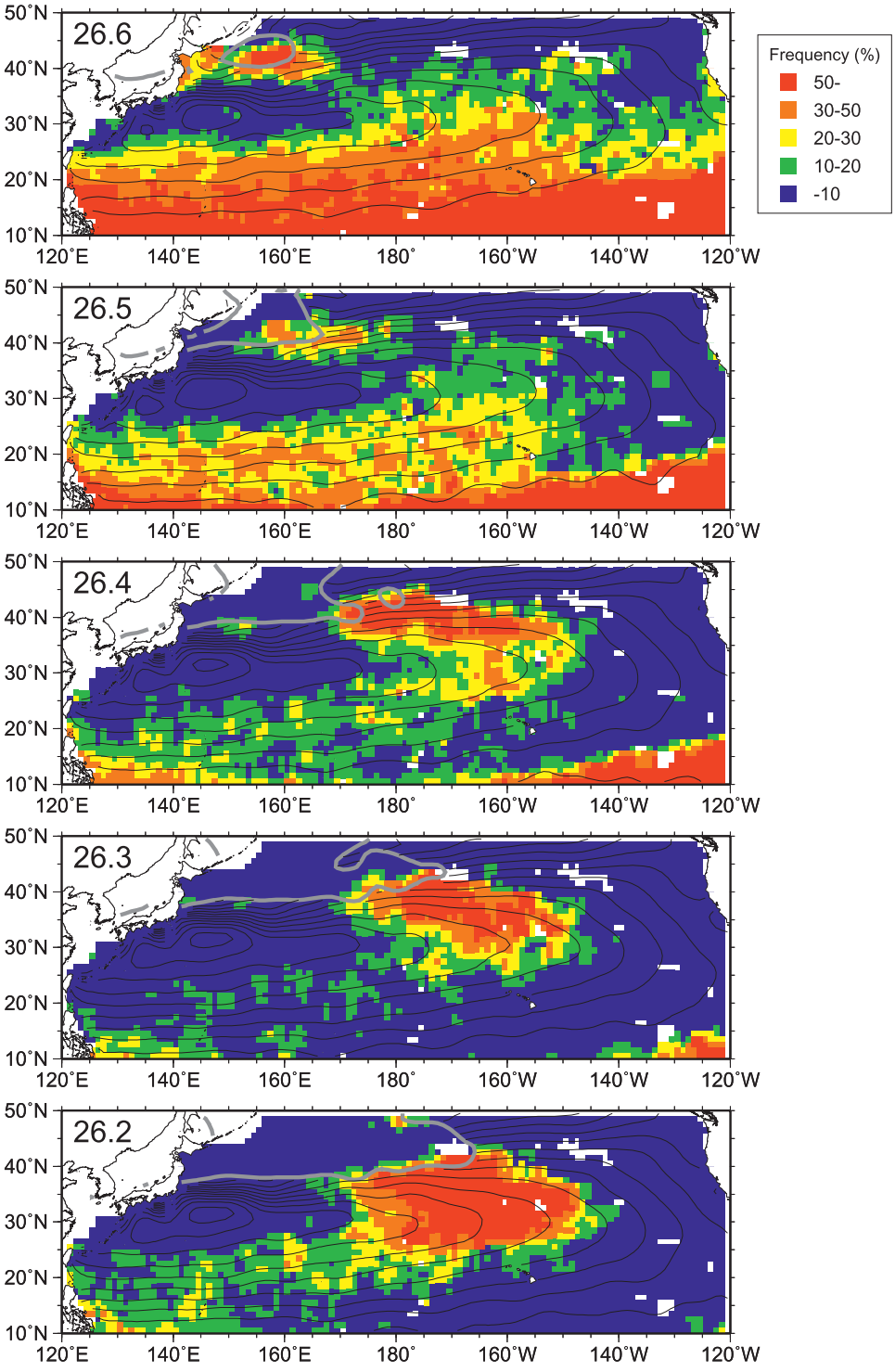

FIG. 9. Frequency of Q lower than a critical value on each isopycnal between $\sigma_\theta = 25.7$ and 26.6 kg m^{-3} (the σ_θ value is given in the top left corner of each panel), based on Argo profiling float data in June–October of 2003–08. The frequency for each $1° \times 1°$ grid box is calculated using the float data in a $3° \times 3°$ grid box centered by the $1° \times 1°$ grid box, only if 10 or more data exist in the $3° \times 3°$ grid box. Critical values of 2.0, 1.75, and 1.5×10^{-10} m^{-1} s^{-1} are used for the isopycnals of σ_θ = 25.7–26.0, 26.1–26.2, and 26.3–26.6 kg m^{-3}, respectively. Thick gray curve denotes the outcrop of each isopycnal in March, and black contours indicate annual-mean acceleration potential relative to 2000 dbar (the contour interval is 0.5 m^2 s^{-2}) on each isopycnal south of the March outcrop, both based on the *World Ocean Atlas 2001* climatology (Conkright et al. 2002).

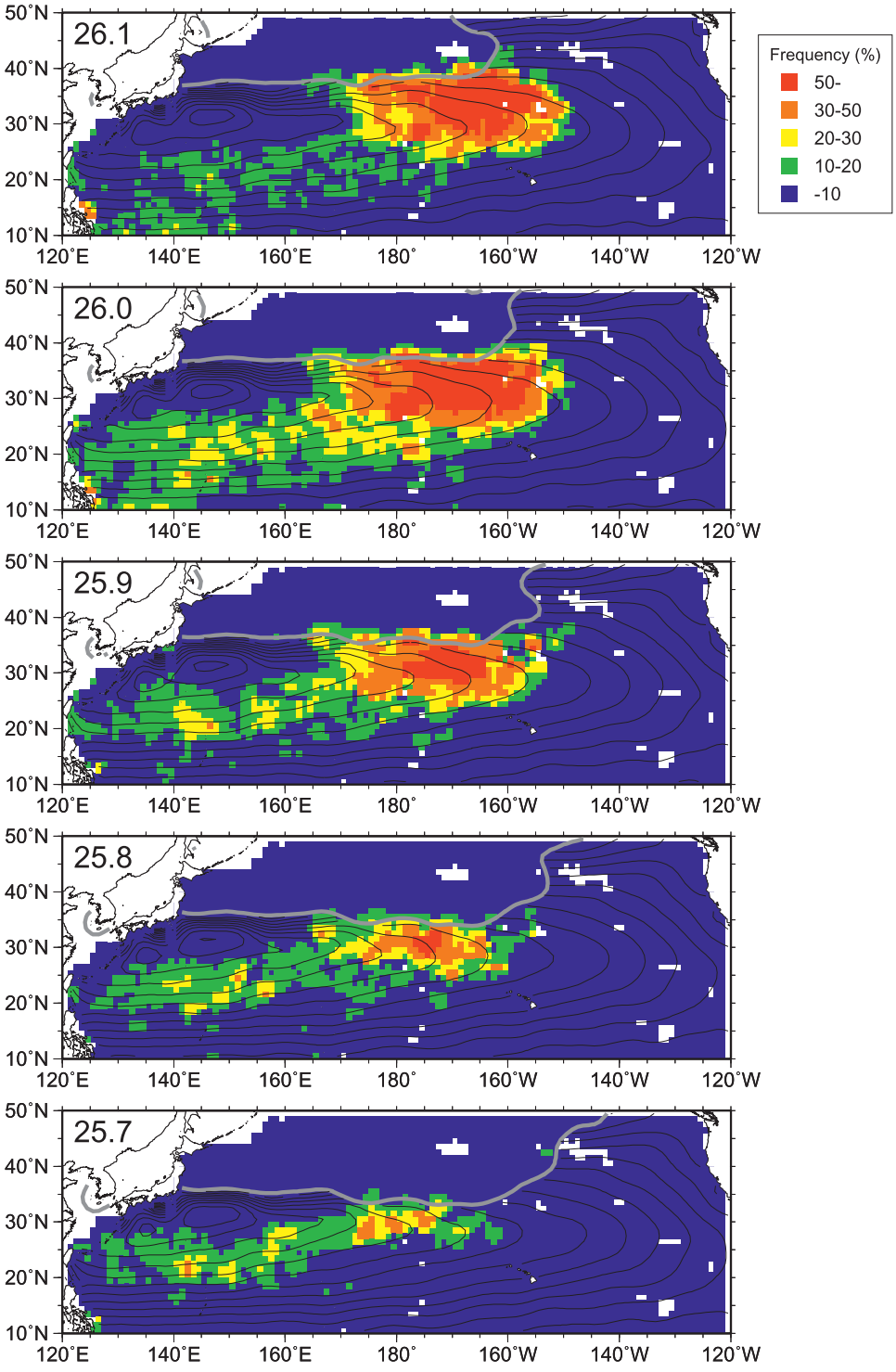

FIG. 9. (*Continued*)

separated by a thermohaline front associated with the northern bifurcation of the Kuroshio Extension (Oka and Suga 2005). However, our analysis has demonstrated that both formation regions extend zonally beyond the longitude range of the Kuroshio bifurcation (approximately between 150°E and 170°W; Levine and White 1983; Mizuno and White 1983; Sainz-Trapaga et al. 2001) to both the west and the east. This might mean that the two zonal

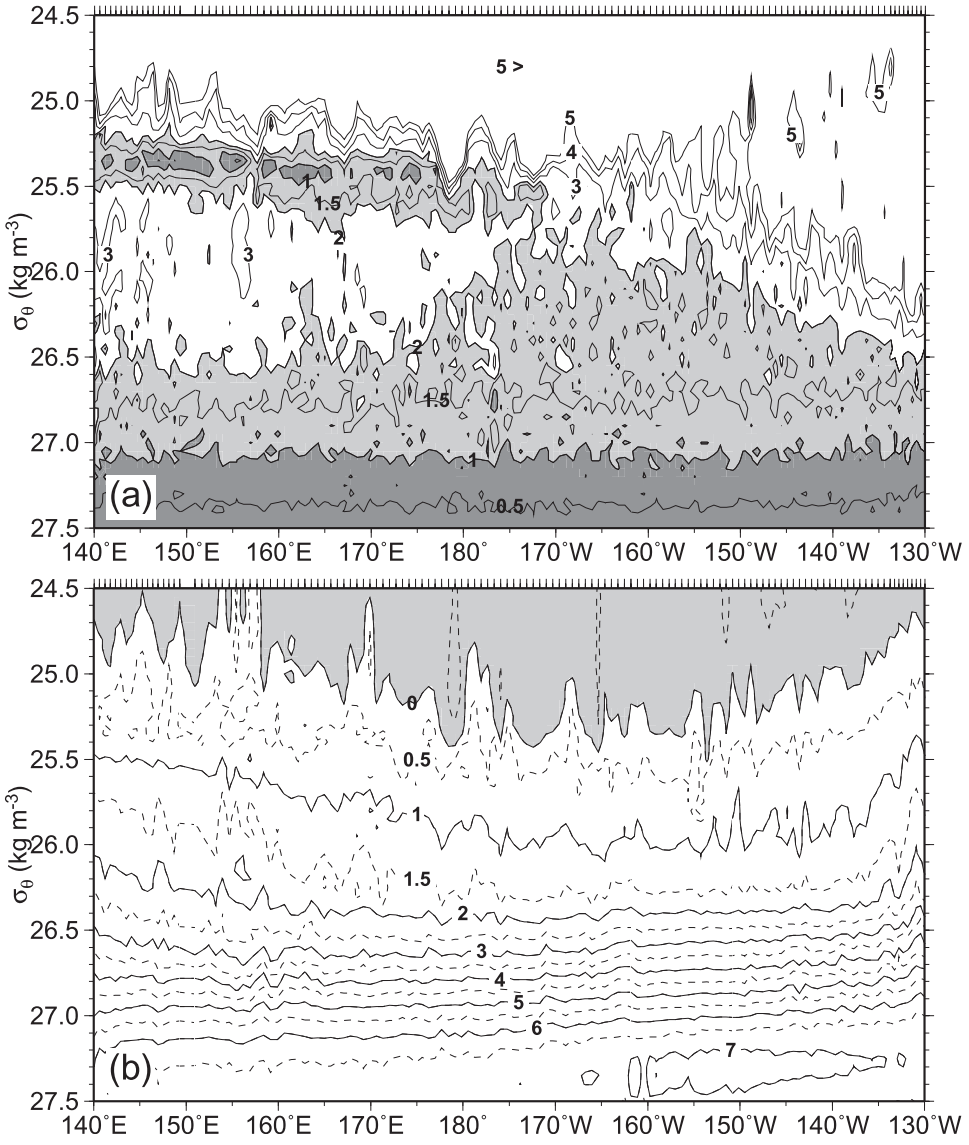

FIG. 10. Distributions of (a) Q (10^{-10} m^{-1} s^{-1}) and (b) AOU (ml l^{-1}) with respect to σ_θ at WHP P02 section along 30°N in June–August 2004. Contours are drawn at 0.5, 1, 1.5, 2, 3, 4, and 5×10^{-10} m^{-1} s^{-1}, and values $<1 \times 10^{-10}$ m^{-1} s^{-1} (of 1–2 $\times$ 10^{-10} m^{-1} s^{-1}) are heavily (lightly) shaded in (a). Negative values are shaded in (b). Tick marks on the top of each panel indicate the $CTDO_2$ stations.

low-Q bands of L-CMW and D-CMW–TRMW in their formation regions are not separated by the Kuroshio bifurcation, as Oka and Suga (2005) speculated, but rather enhance the bifurcation. If, for example, an L-CMW pycnostad with σ_θ of 26.0 kg m^{-3} and a D-CMW pycnostad with 26.4 kg m^{-3} are aligned at similar depths in a meridional section, the isopycnals of σ_θ = 26.1–26.3 kg m^{-3}, which passes below the L-CMW pycnostad to the south and above the D-CMW pycnostad to the north, should shallow sharply northward between the two pycnostads, leading to the generation of an eastward flow. In fact, the longitude range of the Kuroshio bifurcation corresponds to that where both L-CMW and D-CMW are thickest (Figs. 7b,c).

Although the formation regions of STMW and the two varieties of CMW are all zonal bands of deep mixed layer with considerable zonal variations of properties (Figs. 4, 5), the subduction to the permanent pycnocline occurs in a quite different manner between these regions. STMW is formed in the recirculation gyre south of the Kuroshio and the Kuroshio Extension, which consists of several anticyclonic circulations (Oka 2009). The STMW formed in each anticyclonic circulation in winter tends to remain in the respective circulation after spring and is mostly

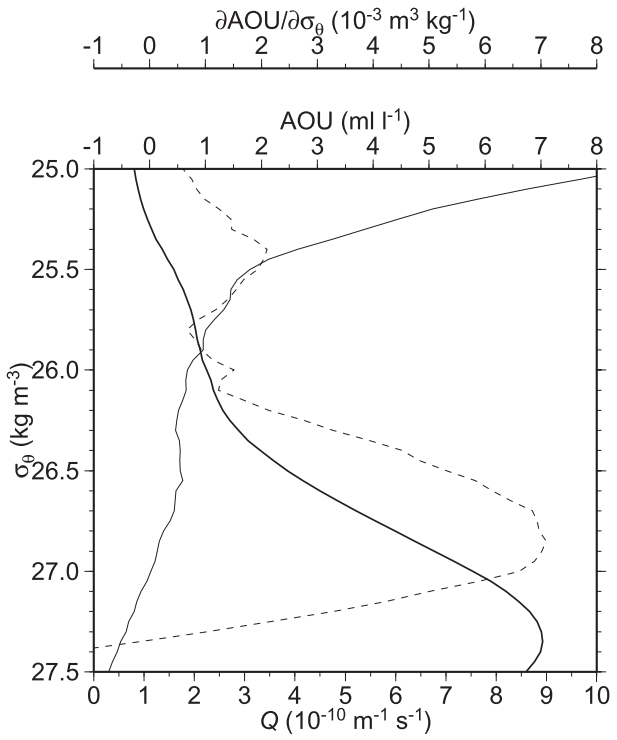

FIG. 11. Vertical profiles of Q (thin solid curve), AOU (thick solid curve), and $\partial \mathrm{AOU}/\partial\sigma_\theta$ (dashed curve) with respect to σ_θ, averaged at 33 $\mathrm{CTDO_2}$ stations between 175° and 155°W at the WHP P02 section.

reentrained into the mixed layer in the following winter, while some portion seeps into the southern region, mainly because of mesoscale activities (Nishikawa et al. 2010), thereby being subducted to the permanent pycnocline. On the other hand, each variety of CMW is advected eastward within the formation region, being "matured" for several years, until it is finally subducted to the permanent pycnocline from the eastern part of the formation region. Such a difference in the "ripening period" suggests that the year-to-year variation of the CMW properties is much smaller than that of the STMW properties, as we assumed in section 1. In fact, the late winter sea surface temperature anomaly in the CMW formation region is highly correlated with that one year later (Hanawa and Sugimoto 2004; Sugimoto and Hanawa 2005).

Nevertheless, decadal and longer time-scale variation of the CMW properties can be large because of changes in the surface heat flux or to meridional shifts of the current system around the CMW formation region (Nonaka et al. 2006). In the subtropical and subarctic North Pacific, several studies reported long-term AOU changes in the subsurface centered at $\sigma_\theta = 26.6$ kg m^{-3} (e.g., Watanabe et al. 2001; Emerson et al. 2004; Mecking et al. 2008), which seem to be characterized by a bidecadal oscillation (Andreev and Kusakabe 2001; Ono et al. 2001). The long-term variations of the CMW subduction scheme and the resultant subduction limit ($\sigma_\theta = 26.4$ kg m^{-3} for 2003–08) might be a cause of such AOU variation. With the accumulated Argo float data for nearly 10 yr, detailed decadal variation of the CMW subduction and circulation, its mechanism, and the associated propagation of temperature and AOU anomalies in the permanent pycnocline shall be the next interesting theme.

In addition to the large-scale, alongfront CMW subduction investigated in this study, eddy-induced, mesoscale CMW subduction is also thought to be important (e.g., Qu et al. 2002). Oka et al. (2009) recently reported a subsurface mesoscale eddy observed at 27.5°N, 145°E in fall 2008, which contains a CMW pycnostad with low AOU indicating that the pycnostad is formed only half a year ago. They speculated that the pycnostad is subducted to the permanent pycnocline in association with the formation of the subsurface mesoscale eddy and its migration across the Kuroshio Extension by the Spall (1995) mechanism, although the reason why the eddy reaches as far south as 27.5°N so quickly is unclear. Such mesoscale subduction can alter the CMW distribution in the subtropical gyre determined by the large-scale subduction, particularly in the σ_θ range of 26.5–26.6 kg m^{-3} in which CMW cannot be subducted to the permanent pycnocline on the large scale, at least for the period of 2003–08. The relative importance of the two types of CMW subduction and its influence on the CMW distribution in the subtropical gyre need to be examined in detail in a future study, in cooperation with high-resolution ocean general circulation models.

Acknowledgments. The authors thank Tsuyoshi Ohira for help in preparing the Argo float data and Sabine Mecking, Hisashi Nakamura, Kensuke Takeuchi, Lynne Talley, Youichi Tanimoto, and an anonymous reviewer for constructive and helpful comments. This work was supported in part by the Japan Society for Promotion of Science [KAKENHI, Grant-in-Aid for Scientific Research (B) 21340133] and the Ministry of Education, Culture, Sports, Science and Technology (MEXT), Japan [Grant-in-Aid for Scientific Research in Priority Areas "Western Pacific Air-Sea Interaction Study (W-PASS)" under Grant 21014004] and by funds from cooperative program (No. 131 in 2007, No. 116 in 2008, and No. 142 in 2009) provided by Ocean Research Institute, The University of Tokyo and the "Studies on Prediction and Application of Fish Species Alteration (SUPRFISH)" sponsored by the Agriculture, Forestry and Fisheries Research Council (AFFRC), Japan. The Argo float data used in this study were collected and made freely available by the International Argo Project and the national programs that contribute to it (available online at http://www.argo.ucsd.edu; http://argo.jcommops.org).

REFERENCES

Akima, H., 1970: A new method of interpolation and smooth curve fitting based on local procedures. *J. ACM,* **17,** 589–603.

Andreev, A. G., and M. Kusakabe, 2001: Interdecadal variability in dissolved oxygen in the intermediate water layer of the western subarctic gyre and Kuril Basin (Okhotsk Sea). *Geophys. Res. Lett.,* **28,** 2453–2456.

Argo Data Management Team, 2009: Argo quality control manual, version 2.5. Argo Data Management, 39 pp.

Bingham, F. M., and T. Suga, 2006: Distributions of mixed layer properties in North Pacific water mass formation areas: Comparison of Argo floats and World Ocean Atlas 2001. *Ocean Sci.,* **2,** 61–70.

Bretherton, F. P., R. E. Davis, and C. B. Fandry, 1976: A technique for objective analysis and design of oceanographic experiment applied to MODE-73. *Deep-Sea Res.,* **23,** 559–582.

Conkright, M. E., R. A. Locarnini, H. E. Garcia, T. D. O'Brien, T. P. Boyer, C. Stephens, and J. I. Antonov, 2002: *World Ocean Atlas 2001: Objective Analysis, Data Statistics, and Figures*. National Oceanographic Data Center, 17 pp.

da Silva, C., C. Young, and S. Levitus, 1994: *Algorithm and Procedures*. Vol. 1, *Atlas of Surface Marine Data 1994,* NOAA Atlas NESDIS 6, 83 pp.

Deser, C., M. A. Alexander, and M. S. Timlin, 1996: Upper-ocean thermal variations in the North Pacific during 1970–1991. *J. Climate,* **9,** 1840–1855.

Dodimead, A. J., F. Favorite, and T. Hirano, 1963: Salmon of the North Pacific Ocean. Part II: Review of oceanography of the subarctic Pacific region. International North Pacific Fisheries Communication, Bull. 13, 195 pp.

Emerson, S., Y. W. Watanabe, T. Ono, and S. Mecking, 2004: Temporal trends in apparent oxygen utilization in the upper pycnocline of the North Pacific: 1980–2000. *J. Oceanogr.,* **60,** 139–147.

Favorite, F., A. J. Dodimead, and K. Nasu, 1976: Oceanography of the subarctic Pacific region, 1960–71. *Bull. Int. North Pac. Comm.,* **33,** 1–187.

Gu, D., and S. G. H. Philander, 1997: Interdecadal climate fluctuations that depend on exchanges between the tropics and extratropics. *Science,* **275,** 805–807.

Hanawa, K., and S. Sugimoto, 2004: 'Reemergence' areas of winter sea surface temperature anomalies in the world's oceans. *Geophys. Res. Lett.,* **31,** L10303, doi:10.1029/2004GL019904.

Hautala, S. L., and D. H. Roemmich, 1998: Subtropical mode water in the northeast Pacific basin. *J. Geophys. Res.,* **103,** 13 055–13 066.

Hosoda, S., S.-P. Xie, K. Takeuchi, and M. Nonaka, 2004: Interdecadal temperature variations in the North Pacific Central Mode Water simulated by an OGCM. *J. Oceanogr.,* **60,** 865–877.

Kara, A. B., P. A. Rochford, and H. E. Hurlburt, 2000: Mixed layer depth variability and barrier layer formation over the North Pacific Ocean. *J. Geophys. Res.,* **105,** 16 783–16 801.

Kubokawa, A., and T. Inui, 1999: Subtropical countercurrent in an idealized ocean GCM. *J. Phys. Oceanogr.,* **29,** 1303–1313.

Ladd, C. A., and L. Thompson, 2000: Formation mechanisms for North Pacific central and eastern subtropical mode waters. *J. Phys. Oceanogr.,* **30,** 868–887.

Latif, M., and T. P. Barnett, 1994: Causes of decadal climate variability over the North Pacific and North America. *Science,* **266,** 634–637.

Levine, E. R., and W. B. White, 1983: Bathymetric influences upon the character of North Pacific fronts, 1976-1980. *J. Geophys. Res.,* **88,** 9617–9625.

Macdonald, A. M., T. Suga, and R. G. Curry, 2001: An isopycnally averaged North Pacific climatology. *J. Atmos. Oceanic Technol.,* **18,** 394–420.

Masuzawa, J., 1969: Subtropical mode water. *Deep-Sea Res.,* **16,** 463–472.

Mecking, S., and M. J. Warner, 2001: On the subsurface CFC maxima in the subtropical North Pacific thermocline and their relation to mode waters and oxygen maxima. *J. Geophys. Res.,* **106,** 22 179–22 198.

——, C. Langdon, R. A. Feely, C. L. Sabine, C. A. Deutsch, and D.-H. Min, 2008: Climate variability in the North Pacific thermocline diagnosed from oxygen measurements: An update based on the U.S. CLIVAR/CO_2 Repeat Hydrography cruises. *Global Biogeochem. Cycles,* **22,** GB3015, doi:10.1029/2007GB003101.

Miura, T., T. Suga, and K. Hanawa, 2002: Winter mixed layer and formation of dichothermal water in the Bering Sea. *J. Oceanogr.,* **58,** 815–823.

Mizuno, K., and W. B. White, 1983: Annual and interannual variability in the Kuroshio Current System. *J. Phys. Oceanogr.,* **13,** 1847–1867.

Nakamura, H., 1996: A pycnostad on the bottom of the ventilated portion in the central subtropical North Pacific: Its distribution and formation. *J. Oceanogr.,* **52,** 171–188.

Nishikawa, S., H. Tsujino, K. Sakamoto, and H. Nakano, 2010: Effects of mesoscale eddies on subduction and distribution of subtropical mode water in an eddy-resolving OGCM of the western North Pacific. *J. Phys. Oceanogr.,* **40,** 1748–1765.

Nonaka, M., S. P. Xie, and K. Takeuchi, 2000: Equatorward spreading of a passive tracer with application to North Pacific interdecadal temperature variations. *J. Oceanogr.,* **56,** 173–183.

——, H. Nakamura, Y. Tanimoto, T. Kagimoto, and H. Sasaki, 2006: Decadal variability in the Kuroshio–Oyashio Extension simulated in an eddy-resolving OGCM. *J. Climate,* **19,** 1970–1989.

Ohno, Y., T. Kobayashi, N. Iwasaka, and T. Suga, 2004: The mixed layer depth in the North Pacific as detected by the Argo floats. *Geophys. Res. Lett.,* **31,** L11306, doi:10.1029/2004GL019576.

——, N. Iwasaka, F. Kobashi, and Y. Sato, 2009: Mixed layer depth climatology of the North Pacific based on Argo observations. *J. Oceanogr.,* **65,** 1–16.

Oka, E., 2009: Seasonal and interannual variation of North Pacific Subtropical Mode Water in 2003–2006. *J. Oceanogr.,* **65,** 151–164.

——, and T. Suga, 2003: Formation region of North Pacific subtropical mode water in the late winter of 2003. *Geophys. Res. Lett.,* **30,** 2205, doi:10.1029/2003GL018581.

——, and ——, 2005: Differential formation and circulation of North Pacific Central Mode Water. *J. Phys. Oceanogr.,* **35,** 1997–2011.

——, ——, and L. D. Talley, 2007: Temporal variability of winter mixed layer in the mid- to high-latitude North Pacific. *J. Oceanogr.,* **63,** 293–307.

——, K. Toyama, and T. Suga, 2009: Subduction of North Pacific central mode water associated with subsurface mesoscale eddy. *Geophys. Res. Lett.,* **36,** L08607, doi:10.1029/2009GL037540.

Ono, T., T. Midorikawa, Y. W. Watanabe, K. Tadokoro, and T. Saino, 2001: Temporal increases of phosphate and apparent oxygen utilization in the subsurface waters of western

subarctic Pacific from 1968 to 1998. *Geophys. Res. Lett.,* **28,** 3285–3288.

Qiu, B., and S. Chen, 2005: Variability of the Kuroshio Extension jet, recirculation gyre and mesoscale eddies on decadal timescales. *J. Phys. Oceanogr.,* **35,** 2090–2103.

——, P. Hacker, S. Chen, K. A. Donohue, D. R. Watts, H. Mitsudera, N. G. Hogg, and S. R. Jayne, 2006: Observations of the subtropical mode water evolution from the Kuroshio Extension System Study. *J. Phys. Oceanogr.,* **36,** 457–473.

Qu, T., S. P. Xie, H. Mitsudera, and A. Ishida, 2002: Subduction of the North Pacific mode waters in a global high-resolution GCM. *J. Phys. Oceanogr.,* **32,** 746–763.

Roden, G. I., 1970: Aspects of the mid-Pacific transition zone. *J. Geophys. Res.,* **75,** 1097–1109.

——, 1972: Temperature and salinity fronts at the boundaries of the subarctic-subtropical transition zone in the western Pacific. *J. Geophys. Res.,* **77,** 7175–7187.

Roemmich, D., and Coauthors, 2001: Argo: The global array of profiling floats. *Observing the Oceans in the 21st Century,* C. J. Koblinsky and N. R. Smith, Eds., Bureau of Meteorology GODAE Project Office, 248–258.

——, and Coauthors, 2009: Argo: The challenge of continuing 10 years of progress. *Oceanography,* **22,** 46–55.

Sainz-Trapaga, S., G. J. Goni, and T. Sugimoto, 2001: Identification of the Kuroshio Extension, its bifurcation and northern branch from altimetry and hydrographic data during October 1992 – August 1999: Spatial and temporal variability. *Geophys. Res. Lett.,* **28,** 1759–1762.

Saito, H., 2006: Transition region mode water of the North Pacific. Ph.D. dissertation, Tohoku University, 114 pp.

——, T. Suga, K. Hanawa, and T. Watanabe, 2007: New type of pycnostad in the western subtropical-subarctic transition region of the North Pacific: Transition region mode water. *J. Oceanogr.,* **63,** 589–600.

Schneider, N., A. J. Miller, M. A. Alexander, and C. Deser, 1999: Subduction of decadal North Pacific temperature anomalies: Observations and dynamics. *J. Phys. Oceanogr.,* **29,** 1056–1070.

Spall, M. A., 1995: Frontogenesis, subduction, and cross-front exchange at upper ocean fronts. *J. Geophys. Res.,* **100,** 2543–2557.

Suga, T., K. Hanawa, and Y. Toba, 1989: Subtropical mode water in the 137°E section. *J. Phys. Oceanogr.,* **19,** 1605–1618.

——, Y. Takei, and K. Hanawa, 1997: Thermostad distribution in the North Pacific subtropical gyre: The central mode water and the subtropical mode water. *J. Phys. Oceanogr.,* **27,** 140–152.

——, K. Motoki, and K. Hanawa, 2003: Subsurface water masses in the central North Pacific transition region: The repeat section along the 180° meridian. *J. Oceanogr.,* **59,** 435–444.

——, ——, Y. Aoki, and A. M. Macdonald, 2004: The North Pacific climatology of winter mixed layer and mode waters. *J. Phys. Oceanogr.,* **34,** 3–22.

——, Y. Aoki, H. Saito, and K. Hanawa, 2008: Ventilation of the North Pacific subtropical pycnocline and mode water formation. *Prog. Oceanogr.,* **77,** 285–297.

Sugimoto, S., and K. Hanawa, 2005: Remote reemergence areas of winter sea surface temperature anomalies in the North Pacific. *Geophys. Res. Lett.,* **32,** L01606, doi:10.1029/2004GL021410.

Takahashi, T., and Coauthors, 2009: Climatological mean and decadal change in surface ocean pCO_2, and net sea–air CO_2 flux over the global ocean. *Deep-Sea Res.,* **56,** 554–577.

Talley, L. D., 1985: Ventilation of the subtropical North Pacific: The shallow salinity minimum. *J. Phys. Oceanogr.,* **15,** 633–649.

——, 1988: Potential vorticity distribution in the North Pacific. *J. Phys. Oceanogr.,* **18,** 89–106.

——, 1993: Distribution and formation of the North Pacific Intermediate Water. *J. Phys. Oceanogr.,* **23,** 517–537.

Tsujino, H., and T. Yasuda, 2004: Formation and circulation of mode waters of the North Pacific in a high-resolution GCM. *J. Phys. Oceanogr.,* **34,** 399–415.

Ueno, H., E. Oka, T. Suga, and H. Onishi, 2005: Seasonal and interannual variability of temperature inversions in the subarctic North Pacific. *Geophys. Res. Lett.,* **32,** L20603, doi:10.1029/2005GL023948.

Watanabe, Y. W., T. Ono, A. Shimamoto, T. Sugimoto, M. Wakita, and S. Watanabe, 2001: Probability of a reduction in the formation rate of the subsurface water in the North Pacific during the 1980s and 1990s. *Geophys. Res. Lett.,* **28,** 3289–3292.

Woods, J. D., 1985: The physics of pycnocline ventilation. *Coupled Ocean-Atmosphere Models,* J. C. J. Nihoul, Ed., Elsevier, 543–590.

Xie, S.-P., T. Kunitani, A. Kubokawa, M. Nonaka, and S. Hosoda, 2000: Interdecadal thermocline variability in the North Pacific for 1958–97: A GCM simulation. *J. Phys. Oceanogr.,* **30,** 2798–2813.

Yasuda, I., 2003: Hydrographic structure and variability of the Kuroshio-Oyashio transition area. *J. Oceanogr.,* **59,** 389–402.

Yasuda, T., and K. Hanawa, 1997: Decadal changes in mode waters in the midlatitude North Pacific. *J. Phys. Oceanogr.,* **27,** 858–870.

Yuan, X., and L. D. Talley, 1996: The subarctic frontal zone in the North Pacific: Characteristics of frontal structure from climatological data and synoptic surveys. *J. Geophys. Res.,* **101,** 16 491–16 508.

Zhang, R.-X., and K. Hanawa, 1993: Features of the water-mass front in the northwestern North Pacific. *J. Geophys. Res.,* **98,** 967–975.